


Static quadrupole moment as a criterion to distinguish chiral modes

B. Hu and Q. B. Chen *

Department of Physics, East China Normal University, Shanghai 200241, China



(Received 30 November 2023; revised 8 January 2024; accepted 22 January 2024; published 7 February 2024)

The static quadrupole moments (SQMs) of multiple chiral doublet bands are investigated. An interesting finding for the SQM is the occurrence of a kink at specific spin values for various γ values. The kink represents the transition point from planar to chiral rotation. This observation highlights a robust feature that the presence of a kink in the SQM plot serves as compelling evidence for the initiation of aplanar rotation. Thus, the SQMs presents a novel criterion for effectively distinguishing different modes of nuclear chirality.

DOI: [10.1103/PhysRevC.109.L021302](https://doi.org/10.1103/PhysRevC.109.L021302)

In 1997, Frauendorf and Meng introduced chirality to nuclear physics [1]. They studied a triaxially deformed rotating nucleus, where the angular momenta align along three principal axes: the intermediate (m), short (s), and long (l) axes. This alignment creates left-handed and right-handed modes, resulting in a spontaneous breaking of chiral symmetry in the body-fixed frame. The broken chiral symmetry is restored in the laboratory frame due to time-reversal invariance and quantum mechanical tunneling of the total angular momentum between both modes. These phenomena allow us to observe chiral doublet bands, which manifest as a pair of nearly degenerate $\Delta I = 1$ bands with the same parity [1]. Up to now, more than 50 candidates for this phenomenon have been observed in the mass regions $A \approx 80, 100, 130$, and 190. For recent reviews on the subject, refer to Refs. [2–9] and the corresponding data tables in Ref. [10]. Significantly, the prediction [11–17] and subsequent confirmations [18–25] of multiple chiral doublet ($M\chi D$) bands within a single nucleus have significantly propelled the investigation of chirality in nuclear structure physics. Correspondingly, various approaches have been developed to investigate the chiral doublet bands. For example, the particle rotor model (PRM) [1,7,26–38] and its approximation solution based on time-dependent variation principle [39–41], the titled axis cranking (TAC) model [42–47], the TAC plus random-phase approximation (RPA) [48], the TAC plus the collective Hamiltonian method [49–51], the interacting boson-fermion model [52], and the angular momentum projection (AMP) method [53–57].

In contrast to $M\chi D$ bands where different partner bands possess distinct triaxial deformations and configurations, the $M\chi D$ phenomenon is also expected with identical configurations [58–61]. This implies that not only the yrast and yrare bands but also higher excited bands may serve as chiral partner bands. The existence of such $M\chi D$ with identical configurations was first observed in the nucleus ^{103}Rh [62], providing evidence that chiral geometry in nuclei can withstand an increase in intrinsic excitation energy. These

significant developments highlight the potential diversity of chiral phenomena in different excitation regimes.

In addition to energy spectra, the measurement of electromagnetic transition strengths plays a pivotal role in identifying nuclear chirality. A theoretical model employing the configuration $\pi(1h_{11/2})^1 \otimes \nu(1h_{11/2})^{-1}$ and a triaxial deformation parameter of $\gamma = 30^\circ$ is commonly utilized for the study of chiral nuclei. The determination of ideal nuclear chirality is based on specific criteria outlined in references, such as Refs. [1,2,5,29,33,34,36,63–70]. These criteria emphasize the importance of observing similarities in the reduced magnetic dipole ($M1$) and electric quadrupole ($E2$) transition strengths both within a specific band (intra-band) and between different bands (inter-band).

Ongoing research is focused on finding additional observables to characterize nuclear chirality. A recent breakthrough involved measuring the g factor in a chiral band, specifically for the band head of ^{128}Cs [71,72]. This measurement provides crucial information about the relative orientations of the particle, hole, and nuclear core angular momentum vectors. The results confirm the prediction of a critical frequency [43,44], where chiral rotation occurs only above a certain value of the rotational frequency. Below this frequency, a planar configuration or chiral vibration [42,73,74] with angular momentum vectors lying within a plane is observed.

In addition, a novel observable, the static (electric) quadrupole moment (SQM), has been extended to study the nuclear chiral doublet bands [38]. The SQM is intricately linked to both the intrinsic deformation parameter, which is a static property characterizing the shape of the nucleus, and the orientation of the total angular momentum, which is a dynamic property reflecting the rotational motion of the nuclear system. The behavior of the SQMs as a function of spin I was analyzed and illustrated for the particle-hole configuration $\pi(1h_{11/2})^1 \otimes \nu(1h_{11/2})^{-1}$ with triaxial deformation parameters ranging from 260° to 270° in the framework of PRM. This investigation represents the first foray into the study of SQMs within the context of chiral nuclear systems. Later on, the SQM has also been employed to investigate the wobbling motion [75,76].

*Corresponding author: qbchen@phy.ecnu.edu.cn

One notes that experimental measurements of the SQMs in relation to chiral rotation are still lacking at present. Currently, such measurements can be done for states with long half-lives like the band heads of some chiral bands, but are not easy to perform for states with short half-lives like those of the collective chiral bands. In spite of this, theoretical study for the SQM in chiral doublet bands is still interesting.

Building upon the previous works, our study aims to expand and enhance the understanding of SQMs in chiral doublet bands. To achieve this, we extend the analysis beyond the yrast states and consider excited doublet bands within a simplified configuration $\pi(1h_{11/2})^1 \otimes \nu(1h_{11/2})^{-1}$. Additionally, we widen the range of triaxial deformation parameters to $240^\circ \leq \gamma \leq 270^\circ$, encompassing a larger span of possible nuclear shapes. An interesting finding of our study for the SQM is the consistent occurrence of a kink with the spin-rotational frequency plot at specific spin values for various γ values. Thus, the SQMs can be considered as a novel criterion for effectively distinguishing different modes of nuclear chirality.

In this work, the calculations are based on the PRM. In the PRM, the Hamiltonian is diagonalized with the total angular momentum I and the projection onto the z axis of the laboratory frame M as good quantum numbers. With the wave function $|I, M = I\rangle$ obtained from PRM, the SQM is calculated as the expectation value of the quadrupole momentum operator \hat{Q}_{20} in the laboratory frame on the state $|II\rangle$ [77],

$$Q(I) = \langle II | \hat{Q}_{20} | II \rangle. \quad (1)$$

The relationship between \hat{Q}_{20} and the intrinsic quadrupole moments $Q'_{2\nu}$ can be expressed as follows:

$$\hat{Q}_{20} = \sum_{\nu} D_{0,\nu}^2 Q'_{2\nu}, \quad (2)$$

where $D_{0,\nu}^2$ are the coefficients of the Wigner D matrix. The components of the intrinsic quadrupole moment $Q'_{2\nu}$ in the principal axis frame are defined as

$$Q'_{20} = Q'_0 \cos \gamma, \quad Q'_{2\pm 1} = 0, \quad Q'_{2\pm 2} = \frac{Q'_0 \sin \gamma}{\sqrt{2}}, \quad (3)$$

in which Q'_0 represents an empirical quadrupole moment.

We can calculate the SQM by considering the following relations between Wigner functions $D_{0,\nu}^2$ and certain angular momentum operators when acting on the states $|II\rangle$ [78],

$$D_{0,0}^2 |II\rangle = \frac{3\hat{I}_3^2 - I(I+1)}{(I+1)(2I+3)} |II\rangle, \quad (4)$$

$$D_{0,2}^2 |II\rangle = \sqrt{\frac{3}{2}} \frac{\hat{I}_+^2}{(I+1)(2I+3)} |II\rangle, \quad (5)$$

$$D_{0,-2}^2 |II\rangle = \sqrt{\frac{3}{2}} \frac{\hat{I}_-^2}{(I+1)(2I+3)} |II\rangle \quad (6)$$

with the raising and lowering operators $\hat{I}_{\pm} = \hat{I}_1 \pm i\hat{I}_2$. As a result, we could decompose the SQM into two components [38]

$$Q(I) = Q_0(I) + Q_2(I), \quad (7)$$

$$Q_0(I) = \frac{3\langle \hat{I}_3^2 \rangle - I(I+1)}{(I+1)(2I+3)} Q'_0 \cos \gamma, \quad (8)$$

$$Q_2(I) = \frac{\sqrt{3}(\langle \hat{I}_+^2 \rangle - \langle \hat{I}_-^2 \rangle)}{(I+1)(2I+3)} Q'_0 \sin \gamma, \quad (9)$$

which can yield valuable insights into the rotational properties of the discussed system.

In our calculations, we consider a system consisting of one proton particle in the $h_{11/2}$ state and one neutron hole in the $h_{11/2}$ state. This system is coupled to a triaxial rigid rotor with quadrupole deformation parameters $\beta = 0.23$ (corresponding to the coupling coefficients $C_p = 0.32$ MeV and $C_n = -0.32$ MeV). The moments of inertia of the irrotational flow type are employed, given by $\mathcal{J}_k = \mathcal{J}_0 \sin^2(\gamma - 2k\pi/3)$ ($k = 1, 2, 3$) with $\mathcal{J}_0 = 30 \hbar^2/\text{MeV}$. For the calculation of the SQM, $Q'_0 = 3.5$ eb is adopted. Note that the total Hamiltonian for the symmetric particle-hole configuration with an irrotational flow type of moment of inertia remains invariant under the transformation $\gamma \rightarrow 540^\circ - \gamma$ ($\gamma \in [240^\circ, 300^\circ]$). This symmetry exchange of angular momentum components along the l and s axes results in SQMs that are symmetric with respect to those obtained at $\gamma = 270^\circ$. Therefore, we will focus on investigating the SQMs within the range of $240^\circ \leq \gamma \leq 270^\circ$. In this context, the triaxially deformed ellipsoid's s , l , and m axes correspond to the one axis, two axis, and three axis, respectively. The moment of inertia \mathcal{J}_m is the largest among the selected γ values, while \mathcal{J}_s is equal to \mathcal{J}_l at $\gamma = 270^\circ$ and slightly larger for other γ values.

In the considered particle-hole configuration $\pi(1h_{11/2})^1 \otimes \nu(1h_{11/2})^{-1}$ and within the triaxial deformation parameters $255^\circ \leq \gamma \leq 285^\circ$ (or equivalently $15^\circ \leq \gamma \leq 45^\circ$), extensive investigations conducted in previous studies [1,33,34,36,38,59,61,66] have comprehensively explored diverse aspects of the system, including energy spectra, electromagnetic transition probabilities, and the underlying angular momentum geometry.

The rotational frequencies $\hbar\omega(I)$ are extracted from the energy spectra $E(I)$ for the four lowest bands (bands 1–4) with a particle-hole configuration of $\pi(1h_{11/2})^1 \otimes \nu(1h_{11/2})^{-1}$ and different triaxial deformation parameters ($\gamma = 265^\circ, 260^\circ, 250^\circ$, and 240°), as shown in Fig. 1. The increase in $\hbar\omega(I)$ values with spin indicates collective rotation enhancement, but a kink is observed, indicating a change in slope and nonmonotonic behavior for some triaxial deformations. The kink occurs at different spins for different γ values. For the lowest band 1, this kink occurs at $I = 14\hbar$ when $\gamma = 265^\circ$, $I = 15\hbar$ when $\gamma = 260^\circ$, and $I = 16\hbar$ when $\gamma = 255^\circ$. For the higher band 3, this kink occurs at $I = 18\hbar$ when $\gamma = 265^\circ$, and at $I = 19\hbar$ when $\gamma = 260^\circ$. However, the kink does not appear in band 1 when $\gamma = 250^\circ$ and 240° . The kink signifies the reorientation of the rotor angular momentum from the l - s plane towards the m axis, resulting in an increase in the dynamical moment of inertia $\mathcal{J}^{(2)}$ [1]. This increase is due to the larger core moment of inertia along the m axis. The kink disappears for smaller γ values, indicating the absence of aplanar rotation. Therefore, the kink serves as evidence for the onset of aplanar rotation, with the kink position being the critical spin at which the rotational mode changes from chiral vibration (planar rotation) to chiral rotation (aplanar rotation), according to Ref. [1].

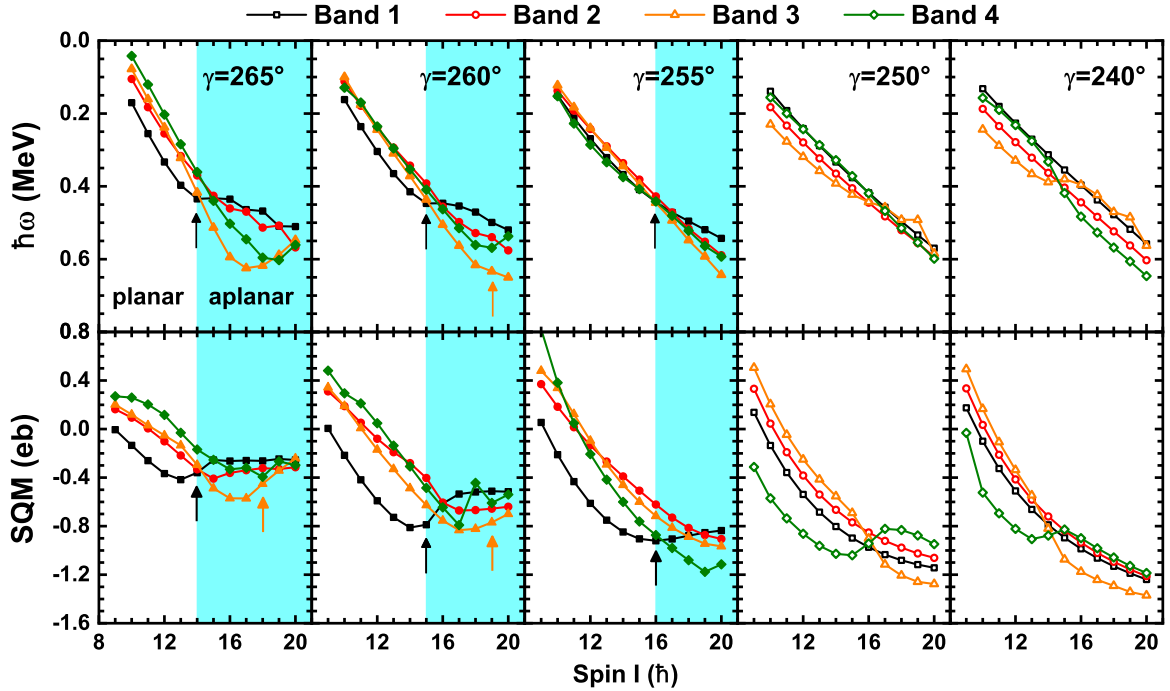


FIG. 1. Rotational frequencies $\hbar\omega(I)$ (upper panels) and static quadrupole moments $Q(I)$ (lower panels) as functions of spin I of the four lowest bands 1–4 calculated in the PRM for the particle-hole configuration $\pi(1h_{11/2})^1 \otimes \nu(1h_{11/2})^{-1}$ with $\gamma = 265^\circ, 260^\circ, 255^\circ, 250^\circ,$ and 240° . Note that the scales of the vertical coordinates in the $\hbar\omega(I)$ plots are inversely shown. The arrows label the kink positions of the $\hbar\omega(I)$ and SQMs plots for bands 1 and 3, while the shadow labels the aplanar rotation region for band 1.

Furthermore, the calculated values of the corresponding SQMs $Q(I)$ for the four lowest bands (bands 1–4) are presented in Fig. 1 for $\gamma = 265^\circ, 260^\circ, 250^\circ,$ and 240° . The results for $\gamma = 270^\circ$ are not included in the figure due to that all SQMs associated with the bands vanish. This occurrence can be attributed to the vanishing of $Q_0(I)$, which is a consequence of the condition $\cos \gamma = 0$. Additionally, the values of $\langle \hat{I}_x^2 \rangle$ and $\langle \hat{I}_y^2 \rangle$ remain equal across the entire range of spin values, leading to the vanishing of $Q_2(I)$. As the triaxial deformation parameter γ deviates from 270° , the corresponding SQMs deviate from zero. Specifically, as γ moves away from 270° , the SQMs transition from positive values at low spin to negative values at higher angular momentum. This behavior reflects the interplay between nuclear structure and rotational motion within the chiral system. The deviation of γ introduces asymmetry, causing distinct changes in the SQMs.

Furthermore, an intriguing observation emerges when examining the behavior of the SQM values in the intermediate-spin region while considering different triaxial deformation parameters, specifically $\gamma = 265^\circ, 260^\circ,$ and 255° . A notable similarity to the $\hbar\omega(I)$ plot shown in Fig. 1 is observed, wherein a kink is present in the $Q(I)$ plot (c.f. Fig. 2 as well). This kink represents a change in the slope of the $Q(I)$ curve. Importantly, the spin value at which the kink appears remains consistent between the two plots. Additionally, as the triaxial deformation parameter γ approaches the prolate deformation value of 240° , the kink disappears. The consistent occurrence of the kink at specific spin values across different values of γ indicates a robust feature that the presence of the kink in the $Q(I)$ plot, similar to the $\hbar\omega(I)$ plot, serves as evidence for the

initiation of aplanar rotation. As expected for $\gamma = 265^\circ$ and 260° , we observe significant distinctions in the behavior of SQMs between the doublet bands, specifically bands 1–2 and bands 3–4, prior to the occurrence of a kink. These disparities can be attributed to the presence of chiral vibrations within the system. The SQM values of band 1 (3) are smaller than those of band 2 (4). On the other hand, we note a similarity in the behavior of SQMs after the kink, indicating the presence of static chirality.

Therefore, we find a strong correlation between the SQM $Q(I)$ and the rotational frequency $\hbar\omega(I)$ in terms of their magnitudes, which are further illustrated in Fig. 2. Specifically, as the value of $Q(I)$ increases, we observe a corresponding decrease in the magnitude of $\hbar\omega(I)$. This finding suggests a significant relationship between $Q(I)$ and $\hbar\omega(I)$, indicating that changes in one variable are accompanied by predictable changes in the other.

In order to gain a more comprehensive understanding of the behavior of SQMs, we conducted an examination of their contributions, denoted as $Q_0(I)$ and $Q_2(I)$, as calculated by Eqs. (8) and (9) for bands 1–4. These contributions are illustrated in Fig. 3. Furthermore, we plot the root mean-square values of the total angular momentum components along the s axis, l axis, and m axis in Fig. 4.

Analysis of Fig. 3 reveals that the suppressive effect of $\cos \gamma$ on $Q_0(I)$ results in its relatively smaller contribution, allowing $Q_2(I)$ to dominate the overall behavior of $Q(I)$. Consequently, the observed decreasing trend of $Q(I)$ in the low-spin region can be attributed to the behavior of $Q_2(I)$. Furthermore, the appearance of a kink in the $Q(I)$ plot is found

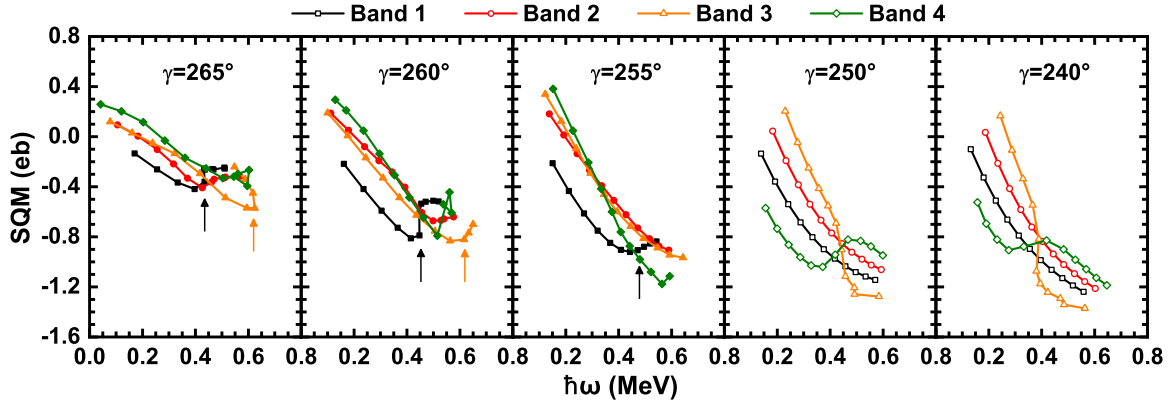


FIG. 2. Static quadrupole moments $Q(I)$ as functions of rotational frequencies $\hbar\omega(I)$ of the four lowest bands 1–4. The arrows label the kink positions of the $\hbar\omega(I)$ and SQMs plots for bands 1 and 3.

to be correlated with the appearance of a kink in the $Q_2(I)$ plot.

The contributions $Q_2(I)$, as described by Eq. (9), arise from the competition between the angular momentum components I_s and I_l . For band 1, I_s is generally larger than I_l due to the selected value of γ , where $\mathcal{J}_s > \mathcal{J}_l$. Consequently, the $Q_2(I)$ contribution for band 1 becomes negative, as $\sin \gamma$ is negative. Notably, a kink is observed in I_s at spin values of $14\hbar$ for $\gamma = 265^\circ$ and $15\hbar$ for $\gamma = 260^\circ$. At these spin values, I_m starts to exceed I_s and I_l . Or in other words, the magnitude of I_m is larger than the mean value of the three-momentum components $\sqrt{I(I+1)/3}$ (cf. Fig. 4) and the corresponding $Q_0(I)$ values become negative (cf. Fig. 3). These observations align with the appearance of a kink in the plots of $\hbar\omega(I)$ and $Q(I)$, providing further evidence for the initiation of aplanar rotation.

For band 2, I_s is marginally smaller than I_l in the region $I \leq 11\hbar$ for $\gamma = 265^\circ$ and 260° . This results in a positive contribution for $Q_2(I)$ and the total $Q(I)$, as depicted in Figs. 1 and 3. However, for $I \geq 12\hbar$, I_s exceeds I_l , akin to the situation observed in band 1, leading to negative SQM values.

For band 3, a kink in I_s is observed at $I = 18\hbar$ for $\gamma = 265^\circ$ and $I = 19\hbar$ for $\gamma = 260^\circ$. This observation is consistent with the corresponding $\hbar\omega(I)$ and $Q(I)$ plots. Furthermore, in the case of band 4, the rise in I_l at $I = 16\hbar$ for $\gamma = 250^\circ$ and $I = 14\hbar$ for $\gamma = 240^\circ$ leads to a sharp kink in the $Q(I)$ plots, as demonstrated in Figs. 1 and 3.

To investigate the influence of configuration on the kinks, we conducted a series of calculations for the $\pi(1g_{9/2})^{-1} \otimes \nu(1h_{11/2})^1$ configuration in the mass region with $A \approx 100$ [68,79,80]. Furthermore, we performed an analysis on the alignment of quasiparticles within the obtained bands. Detailed results can be found in the Supplemental Material accompanying this paper [81]. Through these results, a distinct kink is observed at certain spin values in both the SQM and the rotational frequencies $\hbar\omega(I)$, further indicating a strong correlation between them.

In summary, we have investigated the SQMs of chiral doublets with the particle-hole configuration $\pi(1h_{11/2})^1 \otimes \nu(1h_{11/2})^{-1}$, considering triaxial deformation parameters between 240° and 270° . We observed a consistent kink in the $Q(I)$ plot at specific spin values across different γ values.

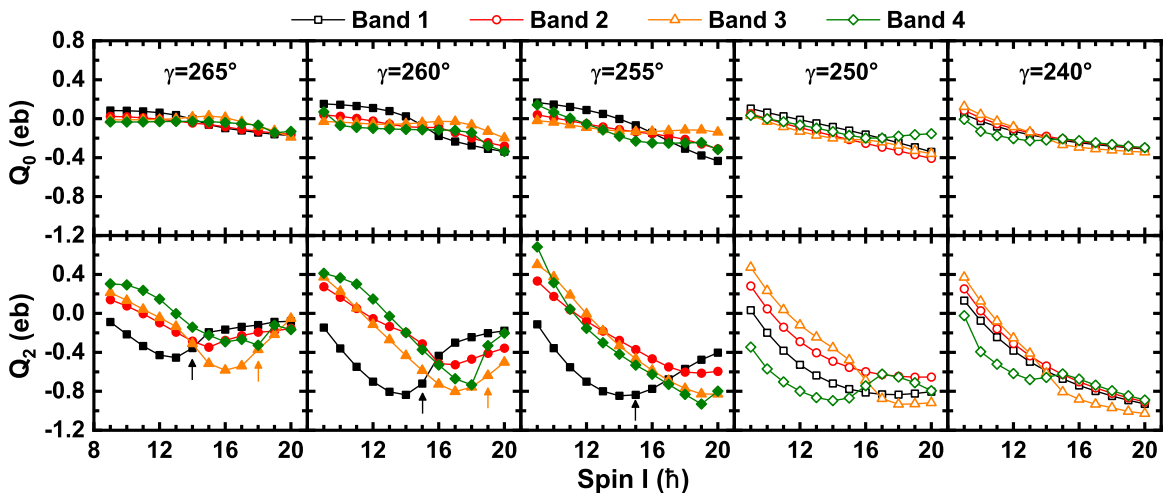


FIG. 3. Contributions to the static quadrupole moment $Q_0(I)$ and $Q_2(I)$ of the four lowest bands 1–4. The arrows label the kink positions of the $Q_2(I)$ plot for bands 1 and 3.

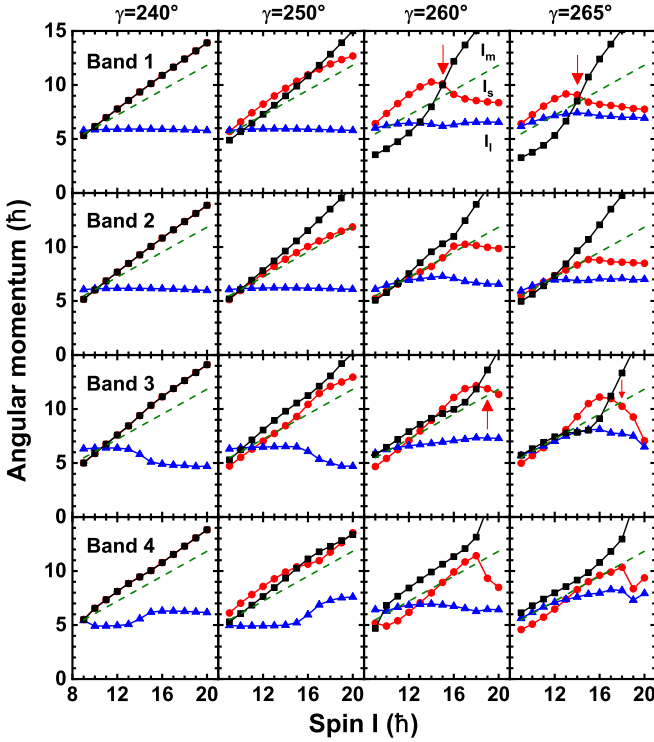


FIG. 4. Root-mean-square values of the total angular momentum components along the short (s , circles), long (l , triangles), and intermediate (m , squares) principal axes for the four lowest bands. The dashed lines represent the average quantity $\sqrt{I(I+1)}/3$. The arrows label the kink positions of the I_s plot for bands 1 and 3.

This observation indicates a robust feature wherein the presence of a kink in the $Q(I)$ plot, similar to the $\hbar\omega(I)$ plot, serves as evidence for the initiation of aplanar rotation.

The kink represents the transition point between planar and chiral rotation. Prior to the kink, significant distinctions in SQM behavior are observed between doublet bands, attributed to the chiral vibrations. After the kink, there was remarkable similarity in SQM behavior, attributed to the static chirality.

The results presented in this work is modeled for the chiral nuclei with the $\pi(1g_{11/2})^1 \otimes \nu(1h_{11/2})^{-1}$ in $A \approx 130$ mass region and $\pi(1g_{9/2})^{-1} \otimes \nu(1h_{11/2})^1$ in the $A \approx 100$ mass regions. Subsequently, it will be interesting to test the model results in the realistic nuclei, for example, the first chiral evidence in the four $N = 75$ isotopes in the $A \approx 130$ mass region [73] or the first chiral candidate in the $A \approx 100$ mass region ^{104}Rh [79] and their neighboring nuclei. However, it is worth noting that in the realistic nucleus, it is possible that at high spin the intrinsic structure might undergoes a change to another configuration and the corresponding SQM can also change. In this case, the band-crossing effect can compete the proposed mechanism of transition from planar to chiral rotation. Further efforts are needed to study the competitions between these two mechanisms.

As discussed earlier, experimental measurements face challenges in accurately measuring the relationship between chiral rotation and SQM properties. One major challenge is the absence of a short-lived radioactive beam for detecting a state with lifetime of less than 50 ns. Additionally, achieving an accuracy better than 10% to detect changes in SQMs is very difficult. To overcome these challenges, future experimental developments are necessary to improve the precision of SQM quantification.

We thank Prof. C. M. Petrache and Prof. J. Srebrny for useful discussions and a careful reading the manuscript. This work was supported by the National Natural Science Foundation of China under Grant No. 12205103.

- [1] S. Frauendorf and J. Meng, *Nucl. Phys. A* **617**, 131 (1997).
- [2] J. Meng and S. Q. Zhang, *J. Phys. G: Nucl. Part. Phys.* **37**, 064025 (2010).
- [3] J. Meng, Q. B. Chen, and S. Q. Zhang, *Int. J. Mod. Phys. E* **23**, 1430016 (2014).
- [4] R. A. Bark, E. O. Lieder, R. M. Lieder, E. A. Lawrie, J. J. Lawrie, S. P. Bvumbi, N. Y. Kheswa, S. S. Ntshangase, T. E. Madiba, P. L. Masiteng *et al.*, *Int. J. Mod. Phys. E* **23**, 1461001 (2014).
- [5] J. Meng and P. W. Zhao, *Phys. Scr.* **91**, 053008 (2016).
- [6] A. A. Raduta, *Prog. Part. Nucl. Phys.* **90**, 241 (2016).
- [7] K. Starosta and T. Koike, *Phys. Scr.* **92**, 093002 (2017).
- [8] S. Frauendorf, *Phys. Scr.* **93**, 043003 (2018).
- [9] Q. B. Chen and J. Meng, *Nucl. Phys. News* **30**, 11 (2020).
- [10] B. W. Xiong and Y. Y. Wang, *At. Data Nucl. Data Tables* **125**, 193 (2019).
- [11] J. Meng, J. Peng, S. Q. Zhang, and S.-G. Zhou, *Phys. Rev. C* **73**, 037303 (2006).
- [12] J. Peng, H. Sagawa, S. Q. Zhang, J. M. Yao, Y. Zhang, and J. Meng, *Phys. Rev. C* **77**, 024309 (2008).
- [13] J. M. Yao, B. Qi, S. Q. Zhang, J. Peng, S. Y. Wang, and J. Meng, *Phys. Rev. C* **79**, 067302 (2009).
- [14] J. Li, S. Q. Zhang, and J. Meng, *Phys. Rev. C* **83**, 037301 (2011).
- [15] J. Peng and Q. B. Chen, *Phys. Rev. C* **98**, 024320 (2018).
- [16] B. Qi, H. Jia, C. Liu, and S. Y. Wang, *Phys. Rev. C* **98**, 014305 (2018).
- [17] J. Li, *Phys. Rev. C* **97**, 034306 (2018).
- [18] A. D. Ayangeakaa, U. Garg, M. D. Anthony, S. Frauendorf, J. T. Matta, B. K. Nayak, D. Patel, Q. B. Chen, S. Q. Zhang, P. W. Zhao *et al.*, *Phys. Rev. Lett.* **110**, 172504 (2013).
- [19] C. Liu, S. Y. Wang, R. A. Bark, S. Q. Zhang, J. Meng, B. Qi, P. Jones, S. M. Wyngaardt, J. Zhao, C. Xu *et al.*, *Phys. Rev. Lett.* **116**, 112501 (2016).
- [20] C. M. Petrache, B. F. Lv, A. Astier, E. Dupont, Y. K. Wang, S. Q. Zhang, P. W. Zhao, Z. X. Ren, J. Meng, P. T. Greenlees *et al.*, *Phys. Rev. C* **97**, 041304(R) (2018).
- [21] T. Roy, G. Mukherjee, M. Asgar, S. Bhattacharyya, S. Bhattacharya, C. Bhattacharya, S. Bhattacharya, T. Ghosh, K. Banerjee, S. Kundu *et al.*, *Phys. Lett. B* **782**, 768 (2018).

- [22] B. F. Lv, C. M. Petrache, Q. B. Chen, J. Meng, A. Astier, E. Dupont, P. Greenlees, H. Badran, T. Calverley, D. M. Cox *et al.*, *Phys. Rev. C* **100**, 024314 (2019).
- [23] C. M. Petrache, B. F. Lv, Q. B. Chen, J. Meng, A. Astier, E. Dupont, K. K. Zheng, P. T. Greenlees, H. Badran, T. Calverley *et al.*, *Eur. Phys. J. A* **56**, 208 (2020).
- [24] S. Guo, C. M. Petrache, D. Mengoni, Y. H. Qiang, Y. P. Wang, Y. Y. Wang, J. Meng, Y. K. Wang, S. Q. Zhang, P. W. Zhao *et al.*, *Phys. Lett. B* **807**, 135572 (2020).
- [25] L. Mu, S. Y. Wang, C. Liu, B. Qi, R. A. Bark, J. Meng, S. Q. Zhang, P. Jones, S. M. Wyngaardt, H. Jia *et al.*, *Phys. Lett. B* **827**, 137006 (2022).
- [26] K. Starosta, C. J. Chiara, D. B. Fossan, T. Koike, T. T. S. Kuo, D. R. LaFosse, S. G. Rohozinski, C. Droste, T. Morek, and J. Srebrny, *Phys. Rev. C* **65**, 044328 (2002).
- [27] T. Koike, K. Starosta, C. J. Chiara, D. B. Fossan, and D. R. LaFosse, *Phys. Rev. C* **67**, 044319 (2003).
- [28] J. Peng, J. Meng, and S. Q. Zhang, *Phys. Rev. C* **68**, 044324 (2003).
- [29] T. Koike, K. Starosta, and I. Hamamoto, *Phys. Rev. Lett.* **93**, 172502 (2004).
- [30] S. Q. Zhang, B. Qi, S. Y. Wang, and J. Meng, *Phys. Rev. C* **75**, 044307 (2007).
- [31] B. Qi, S. Q. Zhang, J. Meng, S. Y. Wang, and S. Frauendorf, *Phys. Lett. B* **675**, 175 (2009).
- [32] E. A. Lawrie and O. Shirinda, *Phys. Lett. B* **689**, 66 (2010).
- [33] Q. B. Chen, K. Starosta, and T. Koike, *Phys. Rev. C* **97**, 041303(R) (2018).
- [34] Q. B. Chen and J. Meng, *Phys. Rev. C* **98**, 031303(R) (2018).
- [35] Q. B. Chen, B. F. Lv, C. M. Petrache, and J. Meng, *Phys. Lett. B* **782**, 744 (2018).
- [36] Q. B. Chen, N. Kaiser, Ulf-G. Meißner, and J. Meng, *Phys. Rev. C* **99**, 064326 (2019).
- [37] Y. Y. Wang, S. Q. Zhang, P. W. Zhao, and J. Meng, *Phys. Lett. B* **792**, 454 (2019).
- [38] Q. B. Chen, N. Kaiser, U.-G. Meißner, and J. Meng, *Phys. Lett. B* **807**, 135568 (2020).
- [39] A. A. Raduta, A. H. Raduta, and C. M. Petrache, *J. Phys. G: Nucl. Part. Phys.* **43**, 095107 (2016).
- [40] R. Budaca, *Phys. Rev. C* **98**, 014303 (2018).
- [41] R. Budaca, *Phys. Lett. B* **797**, 134853 (2019).
- [42] V. I. Dimitrov, S. Frauendorf, and F. Dönau, *Phys. Rev. Lett.* **84**, 5732 (2000).
- [43] P. Olbratowski, J. Dobaczewski, J. Dudek, and W. Płóciennik, *Phys. Rev. Lett.* **93**, 052501 (2004).
- [44] P. Olbratowski, J. Dobaczewski, and J. Dudek, *Phys. Rev. C* **73**, 054308 (2006).
- [45] P. W. Zhao, *Phys. Lett. B* **773**, 1 (2017).
- [46] J. Peng and Q. B. Chen, *Phys. Lett. B* **810**, 135795 (2020).
- [47] J. Peng and Q. B. Chen, *Phys. Rev. C* **105**, 044318 (2022).
- [48] D. Almed, F. Dönau, and S. Frauendorf, *Phys. Rev. C* **83**, 054308 (2011).
- [49] Q. B. Chen, S. Q. Zhang, P. W. Zhao, R. V. Jolos, and J. Meng, *Phys. Rev. C* **87**, 024314 (2013).
- [50] Q. B. Chen, S. Q. Zhang, P. W. Zhao, R. V. Jolos, and J. Meng, *Phys. Rev. C* **94**, 044301 (2016).
- [51] X. H. Wu, Q. B. Chen, P. W. Zhao, S. Q. Zhang, and J. Meng, *Phys. Rev. C* **98**, 064302 (2018).
- [52] S. Brant, D. Tonev, G. de Angelis, and A. Ventura, *Phys. Rev. C* **78**, 034301 (2008).
- [53] G. H. Bhat, J. A. Sheikh, and R. Palit, *Phys. Lett. B* **707**, 250 (2012).
- [54] G. H. Bhat, R. N. Ali, J. A. Sheikh, and R. Palit, *Nucl. Phys. A* **922**, 150 (2014).
- [55] F. Q. Chen, Q. B. Chen, Y. A. Luo, J. Meng, and S. Q. Zhang, *Phys. Rev. C* **96**, 051303(R) (2017).
- [56] M. Shimada, Y. Fujioka, S. Tagami, and Y. R. Shimizu, *Phys. Rev. C* **97**, 024319 (2018).
- [57] Y. K. Wang, F. Q. Chen, P. W. Zhao, S. Q. Zhang, and J. Meng, *Phys. Rev. C* **99**, 054303 (2019).
- [58] C. Droste, S. G. Rohozinski, K. Starosta, L. Próchniak, and E. Grodner, *Eur. Phys. J. A* **42**, 79 (2009).
- [59] Q. B. Chen, J. M. Yao, S. Q. Zhang, and B. Qi, *Phys. Rev. C* **82**, 067302 (2010).
- [60] I. Hamamoto, *Phys. Rev. C* **88**, 024327 (2013).
- [61] H. Zhang and Q. B. Chen, *Chin. Phys. C* **40**, 024102 (2016).
- [62] I. Kuti, Q. B. Chen, J. Timár, D. Sohler, S. Q. Zhang, Z. H. Zhang, P. W. Zhao, J. Meng, K. Starosta, T. Koike *et al.*, *Phys. Rev. Lett.* **113**, 032501 (2014).
- [63] E. Grodner, J. Srebrny, A. A. Pasternak, I. Zalewska, T. Morek, C. Droste, J. Mierzejewski, M. Kowalczyk, J. Kownacki, M. Kisielinski *et al.*, *Phys. Rev. Lett.* **97**, 172501 (2006).
- [64] D. Tonev, G. de Angelis, P. Petkov, A. Dewald, S. Brant, S. Frauendorf, D. L. Balabanski, P. Pejovic, D. Bazzacco, P. Bednarczyk *et al.*, *Phys. Rev. Lett.* **96**, 052501 (2006).
- [65] S. Mukhopadhyay, D. Almed, U. Garg, S. Frauendorf, T. Li, P. V. MadhusudhanaRao, X. Wang, S. S. Ghugre, M. P. Carpenter, S. Gros, A. Hecht, R. V. F. Janssens, F. G. Kondev, T. Lauritsen, D. Seweryniak, S. Zhu, *Phys. Rev. Lett.* **99**, 172501 (2007).
- [66] B. Qi, S. Q. Zhang, S. Y. Wang, J. M. Yao, and J. Meng, *Phys. Rev. C* **79**, 041302(R) (2009).
- [67] E. Grodner, I. Sankowska, T. Morek, S. G. Rohozinski, C. Droste, J. Srebrny, A. A. Pasternak, M. Kisielinski, M. Kowalczyk, J. Kownacki *et al.*, *Phys. Lett. B* **703**, 46 (2011).
- [68] D. Tonev, M. S. Yavahchova, N. Goutev, G. de Angelis, P. Petkov, R. K. Bhowmik, R. P. Singh, S. Muralithar, N. Madhavan, R. Kumar *et al.*, *Phys. Rev. Lett.* **112**, 052501 (2014).
- [69] E. O. Lieder, R. M. Lieder, R. A. Bark, Q. B. Chen, S. Q. Zhang, J. Meng, E. A. Lawrie, J. J. Lawrie, S. P. Bvumbi, N. Y. Kheswa *et al.*, *Phys. Rev. Lett.* **112**, 202502 (2014).
- [70] N. Rather, P. Datta, S. Chattopadhyay, S. Rajbanshi, A. Goswami, G. H. Bhat, J. A. Sheikh, S. Roy, R. Palit, S. Pal *et al.*, *Phys. Rev. Lett.* **112**, 202503 (2014).
- [71] E. Grodner, J. Srebrny, C. Droste, L. Próchniak, S. G. Rohoziński, M. Kowalczyk, M. Ionescu-Bujor, C. A. Ur, K. Starosta, T. Ahn *et al.*, *Phys. Rev. Lett.* **120**, 022502 (2018).
- [72] E. Grodner, M. Kowalczyk, M. Kisieliński, J. Srebrny, L. Próchniak, C. Droste, S. G. Rohoziński, Q. B. Chen, M. Ionescu-Bujor, C. A. Ur *et al.*, *Phys. Rev. C* **106**, 014318 (2022).
- [73] K. Starosta, T. Koike, C. J. Chiara, D. B. Fossan, D. R. LaFosse, A. A. Hecht, C. W. Beausang, M. A. Caprio, J. R. Cooper, R. Krücken *et al.*, *Phys. Rev. Lett.* **86**, 971 (2001).
- [74] K. Starosta, T. Koike, C. J. Chiara, D. B. Fossan, and D. R. LaFosse, *Nucl. Phys. A* **682**, 375 (2001).

- [75] Q. B. Chen, S. Frauendorf, N. Kaiser, U.-G. Meißner, and J. Meng, *Phys. Lett. B* **807**, 135596 (2020).
- [76] C. Broocks, Q. B. Chen, N. Kaiser, and U.-G. Meißner, *Eur. Phys. J. A* **57**, 161 (2021).
- [77] A. Bohr and B. R. Mottelson, *Nuclear Structure*, Vol. II (Benjamin, New York, 1975).
- [78] E. R. Marshalek, *Nucl. Phys. A* **275**, 416 (1977).
- [79] C. Vaman, D. B. Fossan, T. Koike, K. Starosta, I. Y. Lee, and A. O. Macchiavelli, *Phys. Rev. Lett.* **92**, 032501 (2004).
- [80] P. Joshi, D. G. Jenkins, P. M. Raddon, A. J. Simons, R. Wadsworth, A. R. Wilkinson, D. B. Fossan, T. Koike, K. Starosta, C. Vaman *et al.*, *Phys. Lett. B* **595**, 135 (2004).
- [81] See Supplemental Material at <http://link.aps.org/supplemental/10.1103/PhysRevC.109.L021302> for the results of $\pi(1g_{9/2})^{-1} \otimes \nu(1h_{11/2})^1$ configuration in the mass region with $A \approx 100$ and the analysis of quasiparticles alignment for the obtained bands, rotational frequencies $\hbar\omega(I)$, SQM, angular momentum components, quasiparticle alignments. The Supplemental Material also contains Refs. [36,68,79,80].